A Multistate Empirical Valence Bond Approach to a Polarizable and Flexible Water Model†

Aaron E. Lefohn, M. Ovchinnikov, and Gregory A. Voth*

Department of Chemistry and Henry Eyring Center for Theoretical Chemistry, 315 S. 1400 E., Rm 2020, University of Utah, Salt Lake City, Utah 84112-0850

Received: January 11, 2001; In Final Form: April 2, 2001

A new polarizable and flexible water potential has been developed based on the multistate empirical valence bond (MS-EVB) method. The model adds a charge-determination step to the simple point charge/flexible (SPC/F) potential. Two models have been developed: one that is polarizable only along the principal axis, and another that is polarizable in both directions within the molecular plane. The two models give nearly identical radial distribution functions (RDF) for the three site−site RDFs in water: oxygen−oxygen, oxygen−hydrogen, and hydrogen−hydrogen. The new model exhibits a liquid structure that is more ordered than SPC/F but is still well matched to experiment. The gas-phase monomer and dimer properties of the polarizable models are much closer to the experimental result than is SPC/F. Experimental condensed phase properties, such as the bond angle, bond length, molecular dipole moment, and total energy, are also reasonably well reproduced. The static dielectric constant and self-diffusion constant of the model with two directions of polarizability are also reasonably accurate. The MS-EVB method is shown to provide a simple approach to including both polarizability and bond flexibility into a water potential.

I. Introduction

The accurate simulation of, for example, ion solvation, aqueous proton transfer reactions, and water at interfaces requires a water model that has both a flexible intramolecular geometry and is electronically polarizable. Although there are reasonable flexible models[1,2] and several polarizable potentials,[3−9] there are very few polarizable and flexible water models.[8−12] The vast majority of water simulations are done with nonpolarizable potentials that take the electronic induction into account in only an average way. The dipole in these models is fixed at an average condensed phase value, typically between 2.4 and 2.6 D. Although this is a reasonable approximation for bulk water, the fact that the gas-phase dipole of the monomer is 1.85 D suggests that the accurate description of heterogeneous aqueous environments will require a polarizable model.

While empirical models now exist for excess proton transport in aqueous solution,[13−15] the inclusion of explicit polarizability has been neglected, in part due to the lack of availability of a simple, efficient, polarizable, and flexible water potential. It was also recently noted that the exclusion of solvent polarizability in acid ionization simulations is a well-known problem but has been almost completely ignored.[16] With the advent of these methods for modeling aqueous acid−base reactions with empirical potentials, as well as increasing interest in the theoretical study of water in heterogeneous environments, an efficient, accurate, polarizable, and flexible model is clearly needed.

The empirical valence bond (EVB) method has been used for quite some time to describe chemical reactions,[17−19] but has only recently been used to describe molecular polarization.[4,5,20] The method assumes that the ground-state potential energy surface (PES) can be obtained from the ground-state energy of an effective multistate (MS-EVB) Hamiltonian

$$\hat{H}(\mathbf{Q}) = \sum_{ij} |i\rangle\, h_{ij}(\mathbf{Q})\, \langle j| \qquad (1)$$

where the matrix elements, $h_{ij}(\mathbf{Q})$, are a function of the set of nuclear degrees of freedom, $\mathbf{Q}$, of the overall molecular system. The EVB states are chosen so that the linear combination of states will span the range of charge distribution required for the problem at hand. The diagonal elements are usually presumed to be directly related to the nuclear degrees of freedom and are represented by familiar force field expressions. For the molecular polarization problem, the diagonal elements represent the energy of each EVB, charge state, and the off-diagonals represent the coupling between the states and therefore define the polarizability.

In earlier works, Borgis and Staib presented a rigid, EVB-polarizable water potential[4] that consisted of four charge states, with the charge sites being distributed in a tetrahedral structure around the oxygen atom. Kim's TAB/10D model[5,21−24] uses ten charge states to describe each water molecule (six realistic quantum states and four fictitious, EVB-like states). Like Borgis' model, Kim's model also incorporates massless charge sites. Both of these models have shown the promise of the EVB approach to describe molecular polarizability, but neither was formulated to include intramolecular flexibility. The goal of the present work is therefore to create a polarizable and flexible water potential.

In this paper, two such water potentials (called Polarflex) are developed. The first model consists of only two EVB states and is polarizable only in the *z* (principal) direction. The second model has three EVB charge states and is polarizable in the *z* and in the *y* direction, where *z* and *y* define the molecular plane (see Figure 1). This paper is organized as follows: section II explains the form of the potential, while section III gives the formulation of the Polarflex algorithm. Section IV gives the computational details of the simulations run for this work, while section V presents the simulation results. Section VI contains concluding remarks.

† Part of the special issue "Bruce Berne Festschrift".

10.1021/jp010103j CCC: $20.00
Published on Web 05/19/2001

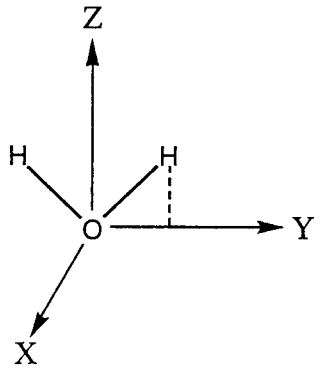

Figure 1. Molecular coordinate system used in the Polarflex model. Note that the plane of the molecule lies in the *YZ* plane.

TABLE 1: SPC/F Intramolecular Water Potential Parameters

parameter	SPC/F	units
ρ_w	2.566	Å^{-1}
D_w	0.708	mdyn Å
r_{OHeq}	1.0	Å
HOH bond angle	109.47	degrees
b	2.283	mdyn Å^{-1}
c	−1.469	mdyn Å^{-1}
d	0.776	mdyn Å^{-1}

TABLE 2: Oxygen−Oxygen Lennard-Jones Parameters for SPC/F Water

ϵ/K_B (K)	(σ Å)
78.22	3.165

II. Model Description

Polarflex water is, at its heart, an SPC/F[1] classical water model that has had an effective charge determination step added to the potential. The pairwise potential is used to determine the forces on each atom and is of the form $V_{\text{Total}} = V_{\text{Intra}} + V_{\text{LJ}} + V_{\text{Coulomb}}$. The intramolecular potential energy is the SPC/F form, i.e., an harmonic potential parameterized by Kutchiso and Morino[1] and is given by

$$V_{\text{Intra}}^{H_2O} = \frac{a}{2}\rho_w^2 D_w (r_{OH_1} - r_{OH_{eq}})^2 + \frac{a}{2}\rho_w^2 D_w (r_{OH_2} - r_{OH_{eq}})^2 + \frac{b}{2}(r_{HH} - r_{HH_{eq}})^2 + c(r_{OH_1} + r_{OH_2} + 2r_{OH_{eq}})(r_{HH} - r_{HH_{eq}}) + d(r_{OH_1} - r_{OH_{eq}})(r_{OH_2} - r_{OH_{eq}}) \quad (2)$$

where r_{ij} is the intramolecular distance from atom i to atom j, and $r_{ij_{eq}}$ is the appropriate equilibrium bond length. All of the bond force constants and equilibrium distances are given in Table 1.

The Lennard-Jones potential energy accounts for both the close-range, intermolecular electron correlation attractions, and the repulsive core that defines the atomic size. The SPC/F model defines only the oxygen sites to have Lennard-Jones interactions. The potential is given by

$$V_{\text{LJ}} = \sum_{i}^{N_o}\sum_{j>i}^{N_o} 4\epsilon_{oo}\left[\left(\frac{\sigma_{oo}}{r_{ij}}\right)^{12} - \left(\frac{\sigma_{oo}}{r_{ij}}\right)^{6}\right] \quad (3)$$

where ϵ_{oo} and σ_{oo} are given in Table 2.

The Coulombic potential energy is the sum of the intermolecular, atomic site, charge−charge interactions and is given by

$$V_{\text{Coulomb}} = \sum_{i}^{N_s}\sum_{j>i}^{N_s}\frac{q_i q_j}{r_{ij}} \quad (4)$$

where N_s is the number of atomic charge sites. The Polarflex algorithm determines these atomic partial charges, q_i, and redefines the strength of V_{Coulomb}. The spatial derivative of eq 4 is used for the Coulombic force contributions. Note that an Ewald summation is used to approximate eq 4 for a condensed phase system due to the finite size of the simulation cell. This is explained more fully in the simulation detail section (section IV) and the Appendix.

III. Polarflex Algorithm

The Coulombic induction is modeled by the Polarflex algorithm with an MS-EVB approach. In the case of Polarflex, a set of charge states that span the molecular polarization space are created. In effect, the Polarflex algorithm replaces eq 4 with $\langle\Psi_0^{\text{EVB}}|\hat{H}_{\text{Coulomb}}|\Psi_0^{\text{EVB}}\rangle$. This section explains both the MS-EVB, Coulombic Hamiltonian and the determination of the EVB "wave function." Both a simple, two-state EVB model with only one direction of polarizability and a more rigorous, three-state model that allows for polarizability in two directions have been developed. The EVB "quantum" states for the two models are shown in Figure 2.

The MS-EVB Hamiltonian matrix for the monomer is "inferred" from experimental gas phase results, namely the dipole moment and polarizability of a water molecule. In the model, point charges are then obtained by the diagonalization of the molecule's MS-EVB, Hamiltonian matrix. The model responds to external electric fields or the field caused by neighboring molecules by self-consistently (SCF) determining the diagonal elements of each molecule's MS-EVB Hamiltonian. It is through this SCF solution that the many-body induction effect is reproduced.

For the sake of clarity, only the three-state Polarflex model will be considered in this section, but the two-state derivation is directly analogous. The derivation of the monomer Hamiltonian matrix for the three-state MS-EVB model first involves finding a symmetry-adapted set of eigenfunctions. Using group theory and orthonormality considerations, one arrives at the general form of the eigenstates,

$$\Phi_0 = -C|0\rangle + \frac{S}{\sqrt{2}}(|1\rangle + |2\rangle) \quad (5)$$

$$\Phi_1 = +S|0\rangle + \frac{C}{\sqrt{2}}(|1\rangle + |2\rangle) \quad (6)$$

$$\Phi_2 = \frac{1}{\sqrt{2}}(|1\rangle - |2\rangle) \quad (7)$$

where $|n\rangle$ refers to the nth EVB basis state shown in Figure 2. To fully characterize the 3×3 molecular Hamiltonian matrix, the energies E_1 and E_2 of the excited states Φ_1 and Φ_2 must be defined (assuming that the energy of the ground state is taken to be $E_0 \equiv 0$). In addition, the coefficients S and C must also be determined. Note that these coefficients are interrelated by $S = \sqrt{1-C^2}$. The full characterization of the monomer Hamiltonian thus requires the determination of three unknowns: E_1, E_2, and C (or S).

The first of three experimental inputs to the model, the z component of the gas-phase dipole of the water monomer, is then used to determine C and S (see Figure 1 for the molecular

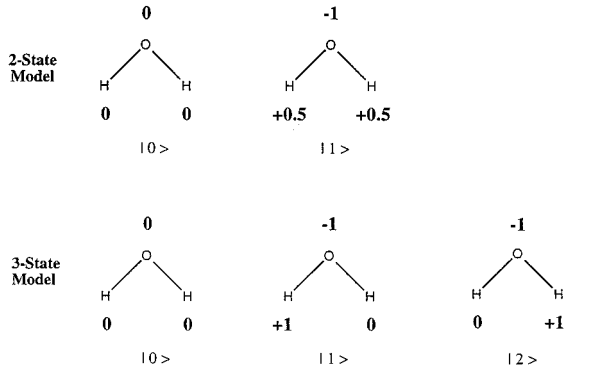

Figure 2. EVB states for the two-state and three-state Polarflex models.

axes). For an isolated monomer, Φ_0 (eq 5) is the complete ground-state wave function and, thus, knowing the expectation value of the dipole operator determines the linear combination coefficients in the following way:

$$\mu_z = \langle \Psi_g | \hat{\mu}_z | \Psi_g \rangle \tag{8}$$

where $\Psi_g = \Phi_0$ and

$$\mu_z = \frac{S^2(\mu_{1z} + \mu_{2z})}{2} \tag{9}$$

determines S, and therefore C. In eq 9, μ_{nz} is the z component of the dipole for EVB state $|n\rangle$, and μ_z is the z component of the experimental dipole moment.

The molecular polarizability tensor, $\boldsymbol{\alpha}$, is defined as the first-order proportionality tensor between an external electric field, $\boldsymbol{\epsilon}$, and the induced dipole, $\boldsymbol{\mu'}$. An expression for each component of the polarizability tensor is derived in terms of the symmetry-adapted basis set, eqs 5−7, by considering the first-order perturbation to the total wave function by an electric field. First, considering the polarizability in the z direction, α_{zz}, analogous to the case of the unperturbed monomer (eq 8), the z component of the total dipole moment for a single water molecule under the influence of an electric field is

$$\mu_z^{\epsilon} = \langle \Psi^{\epsilon} | \hat{\mu} | \Psi^{\epsilon} \rangle \tag{10}$$

where instead of $\Psi = \Phi_0$,

$$|\Psi^{\epsilon}\rangle = |\Phi_0\rangle + \sum_{n=1,2} \frac{\langle \Phi_n | \mu_z \epsilon_z | \Phi_0 \rangle}{E_n} |\Phi_n\rangle + ... \tag{11}$$

Due to symmetry considerations, eq 10 can be simplified to

$$\mu_z^{\epsilon} = \mu_z^0 + 2\frac{\langle \Phi_1 | \hat{\mu}_z | \Phi_0 \rangle \langle \Phi_0 | \hat{\mu}_z | \Phi_1 \rangle}{E_1} \epsilon_z \tag{12}$$

which is of the form, $\mu_z^{\epsilon} = \mu_z^0 + \alpha_{zz}\epsilon_z$. The expression for α_{zz} is thus

$$\alpha_{zz} = 2\frac{\langle \Phi_1 | \hat{\mu}_z | \Phi_0 \rangle \langle \Phi_0 | \hat{\mu}_z | \Phi_1 \rangle}{E_1} \tag{13}$$

Since the dipoles of the EVB states are known constants, eq 13 reduces to

$$\alpha_{zz} = \frac{C^2 S^2 (\mu_{1z} + \mu_{2z})^2}{2E_1} \tag{14}$$

where μ_{nz} is the z component of the permanent dipole of the nth EVB state.

An exactly analogous derivation involving an electric field in the y direction leads to an expression for α_{yy} of

$$\alpha_{yy} = \frac{S^2 (\mu_{1y} + \mu_{2y})^2}{2E_2} \tag{15}$$

and

$$\alpha_{xx} = 0 \tag{16}$$

Note that because SPC water models have only partial charges located on their atomic sites, there is no out-of-plane molecular polarizability, α_{xx}, in the current Polarflex model. Using the components of the experimental polarizability tensor as input into eqs 14 and 15, E_1 and E_2 are now specified and the Hamiltonian matrix for the symmetry-adapted diagonal set, given by

$$\mathbf{H}_{\mathrm{M}}^{(0)} = \begin{pmatrix} E_0 & 0 & 0 \\ 0 & E_1 & 0 \\ 0 & 0 & E_2 \end{pmatrix} \tag{17}$$

has now been fully characterized. The subscript M in the above expression denotes that the matrix is an unperturbed single molecule Hamiltonian, and the superscript (0) indicates the symmetry-adapted basis.

The symmetric Hamiltonian matrix for the MS-EVB basis set, given by

$$\mathbf{H}_{\mathrm{M}} = \begin{pmatrix} V_{00} & V_{01} & V_{02} \\ V_{01} & V_{11} & V_{12} \\ V_{02} & V_{12} & V_{22} \end{pmatrix} \tag{18}$$

is obtained from eq 17 via the similarity transform,

$$V_{nm}^{\mathrm{EVB}} = \langle n | \left[\sum_{i=0}^{2} |\Phi_i\rangle E_i \langle \Phi_i | \right] | m \rangle \tag{19}$$

This results in the following parameterization equations for the MS-EVB Hamiltonian in terms of the diagonal Hamiltonian elements:

$$V_{00} = S^2 E_1$$

$$V_{11} = V_{22} = \frac{1}{2}(C^2 E_1 + E_2)$$

$$V_{02} = V_{01} = \frac{SC}{\sqrt{2}} E_1$$

$$V_{12} = \frac{1}{2}(C^2 E_1 - E_2) \tag{20}$$

In summary, the gas phase Hamiltonian matrix for a single, Polarflex water molecule, described by the three-state MS-EVB basis set shown in Figure 2, has been completely characterized by *defining* that the matrix elements are a result of the single molecule dipole moment and polarizability. It should be noted that the latter quantity will not in general equal the experimental

TABLE 3: Gas Phase, Coulombic Hamiltonian Matrix Elements for the Polarflex Water Models, Two-state Polarflex (2S−PF), and Three-state Polarfelx (3S−PF)

matrix element	2S−PF	3S−PF
V_{00}	0.064733	0.066828
$V_{11} = V_{22}$	0.032299	0.254471
$V_{01} = V_{02}$	0.045726	0.034192
V_{12}		−0.21948

All energies are in hartrees.

TABLE 4: Gas Phase Dipole and Molecular Polarizability Input Parameters for the Polarflex Models

input parameter	2S−PF	3S−PF	exp.	units
μ_z	1.85	1.85	1.85[a]	Debye
α_{zz}	0.8074	0.8074	1.468[b]	Å^3
α_{yy}	0.0	0.8404	1.528[b]	Å^3
α_{xx}	0.0	0.0	1.415[b]	Å^3

[a] Reference 25. [b] Reference 26.

gas-phase polarizability because of the limitations of the underlying SPC model.

As was mentioned above, an analogous derivation can be used to derive the Hamiltonian matrix elements for the two-state Polarflex model. The results from this derivation are shown in eq 21 and 22 below:

$$\mu_z = \mu_{1z} S^2$$

$$\alpha_{zz} = \frac{2C^2 S^2 \mu_{1z}^2}{E_1}$$

$$\alpha_{yy} = \alpha_{xx} = 0 \tag{21}$$

and eq 22

$$V_{00} = S^2 E_1$$

$$V_{11} = C^2 E_1$$

$$V_{01} = CSE_1 \tag{22}$$

The parameters used in the current work for the Hamiltonian matrix elements for both models are given in Table 3. Note that these values are specific to both the MS-EVB charge states and the monomer geometry. Table 4 gives the dipole[25] and polarizability[26] used as input for the Polarflex model. Again, it should be noted here that, although the experimental dipole moment is used for the Polarflex parametrization, a reduced molecular polarizability has been used. An explanation for the use of an altered polarizability will be discussed in section V.

For a given external perturbation, the diagonalization of the MS-EVB matrix gives the ground state, single molecule wave function, Ψ_g, and the effective atomic partial charges, q_i, are determined by

$$q_i = \sum_{n=0}^{N-1} c_n^2 \langle n|\hat{q}_i|n\rangle \tag{23}$$

where N is the number of MS-EVB states for a single molecule, i is the atomic site number ($i = 1 \rightarrow 3$ for water), c_n are the linear combination coefficients that make up Ψ_g, and $\langle n|\hat{q}_i|n\rangle$ is defined as the charge on site i in MS-EVB basis state $|n\rangle$ (from here on, abbreviated as q_i^n).

Up to this point only a single, isolated, gas-phase water molecule has been considered. In order for the algorithm to take into account the electric field produced by neighboring molecules or an external electric field, the Coulombic potential energy of the entire system must be added to the diagonal elements of the Polarflex Hamiltonian matrix, **H**. Making the approximation that a single water molecule is surrounded by fixed point charges, this electric field perturbation for each state of molecule I is given by

$$\mathbf{H}_{nn} = (\mathbf{H}_M)_{nn} + \sum_{i=1}^{3} q_i^n \mathrm{EP}_i \tag{24}$$

where $(\mathbf{H}_M)_{nn}$ refers to the isolated monomer value (eq 18), and

$$\mathrm{EP}_i = \sum_{j=1}^{N_s} \frac{q_j}{r_{ij}} \tag{25}$$

where EP_i is the electrostatic potential at site i. Note that eq 25 is strictly an intermolecular sum, i.e., the index runs over all sites on all molecules other than molecule I. The off-diagonal elements of the molecular Hamiltonian remain unchanged.

In an ensemble of N_{mol} water molecules, the total basis consists of $N \times N_{mol}$ MS-EVB states, where N is the number of MS-EVB states per molecule. To avoid the diagonalization of the very large $(N \times N_{mol})^2$ matrix, the self-consistent field (SCF) method is used to approximate the ground state of the system. Each molecule's Coulombic terms in its Hamiltonian are considered separately, and all other molecules are assumed to be in their previously assigned superposition of MS-EVB states. The diagonalization of each molecular Hamiltonian leads to new ground-state wave functions, Ψ_I, from which the average charges, q_i, are determined. The calculation is then iterated until the system energy stays constant within a set tolerance (1×10^{-9} relative energy difference). The total potential energy for a system of Polarflex water molecules is then given by

$$V_{sys} = \sum_{I=1}^{N_{mol}} \langle \Psi_I^g | \hat{H}_M | \Psi_I^g \rangle + \sum_{i=1}^{N_s - 1} \sum_{j>i}^{N_s} \frac{q_i q_j}{r_{ij}} + \sum_{i=1}^{N_{mol}} V_{intra}^{H_2O} + V_{LJ} \tag{26}$$

The first term in this expression represents the work of polarization, and the second term is the total Coulombic potential energy of the system. Alternative but equivalent expressions for the MS-EVB energy terms can be found in ref 5.

IV. Simulation Details

All condensed phase simulations were performed with 256 water molecules, a time step of 0.5 fs, a density of 1.0 g/cm^3, and at a temperature of 300 K. For the Polarflex simulations, all waters were given a gas phase, initial charge distribution and allowed to equilibrate to their local electric field environment. The Verlet algorithm[27] was used to solve the Newtonian equations of motion. Cubic, minimum imaging of all atomic coordinates was done for all distance calculations, but periodic boundary conditions were not applied to the absolute coordinates so that diffusion constants could be calculated. A radial cutoff the size of half of the box length ($L/2 = 9.86$ Å) was used for all real space potential and force calculations. The length scale of Coulombic interactions, however, is too large to fit into the typical size of a simulation cell. To accurately account for this, the Ewald summation technique was utilized to calculate the long-range potential and forces. This method assumes that the system is infinitely periodic in all directions and calculates the

TABLE 5: Properties of the SPC/F, Two-State Polarflex (2S−PF), and Three-State Polarflex (3S−PF) Water Models as Well as the Experimental Values

	SPC/F	2S−PF	3S−PF	exp.	units
			Monomer		
dipole	2.3	1.85	1.85	1.85[a]	Debye
bond angle	109.47	109.47	109.47	104.52[b]	degrees
bond length	1.0	1.0	1.0	0.957[b]	Å
			Dimer		
energy	−6.8	−4.6	−4.8	−5.4[c]	kcal/mol
OO distance	2.74	2.83	2.78	2.98[c]	Å
			Condensed Phase		
total energy	−11.5	−10.5	−10.5	−10.0[d]	kcal/mol
dipole	2.42	2.55	2.55	2.4−2.6[e]	Debye
bond angle	105.7	105.2	105.2	104−108[f]	degrees
bond length	1.02	1.02	1.02	0.970[f]	Å
ϵ_0	80 ± 8[i]	98 ± 10	85 ± 10	78.3[g]	
ϵ_∞	1	1.11	1.23	1.79[g]	
diffusion constant	3.0[i]	1.5	1.9	2.3[h]	$\times 10^{-9}$ m^2 s

[a] Reference 25. [b] Reference 40. [c] Reference 41. [d] Reference 42. [e] Reference 43. [f] Reference 44. [g] Reference 45. [h] Reference 46. [i] Reference 31.

Coulomb interactions over all cells via a Fourier-space summation. Details of the algorithm for the Polarflex model are given in the Appendix.

All simulations were allowed to equilibrate for at least 50 ps in the canonical ensemble before data collection began, and all data were collected in the microcanonical ensemble unless otherwise specified. Canonical ensemble runs were kept at 300 K $\pm$ 0.75 K via a simple, velocity-scaling thermostat. The scaling is such that if the target temperature, T_0, is 300 K and the trajectory-averaged temperature is T, then the new velocities are scaled by

$$v_i' = v_i \sqrt{\frac{T_o}{T}} \tag{27}$$

in order to maintain T at T_0 on average.

Polarflex water simulations with the SCF algorithm are roughly four times slower than for SPC/F water. The Polarflex algorithm can be encapsulated into a single function call so that it can easily be added to any existing molecular dynamics simulation that uses an array for atomic site charges.

V. Results and Discussion

A. Model Properties. Table 5 shows the values for monomer, dimer, and liquid phase properties for all three water models as well as experiment. The SPC/F model, like all nonpolarizable water models, is bound to give the incorrect result for the monomer and dimer since the dipole moment is fixed and parameterized for the condensed phase. The Polarflex models, however, are parameterized to give the correct gas-phase dipole moment, hence the perfect agreement with the experimental value is not a surprise. The polarizable results for the dimer energy and geometry show a considerable improvement over the nonpolarizable model. Note that by using the condensed phase values for the dipole, SPC/F dramatically overestimates binding energy and underestimates the oxygen−oxygen distance.

The liquid phase results for the Polarflex models seem promising. The total binding energy deviates only 0.5 kcal/mol from the experimental value, whereas the SPC/F value is 1.5 kcal/mol too low. Even though the dipoles are higher in the polarizable models, about 0.1 D higher than in SPC/F, the total binding energy is weaker because the work required to polarize the individual water molecules is included. Note that the Polarflex dipoles are the result of the water molecules polarizing all the way from a gas phase charge distribution. It must be noted here that, as Table 4 shows, the input polarizability values are 55% of the experimental numbers. As can be seen from the derivation in section III, the polarizability is a parameter and not a result of the Polarflex model. The components of the polarizability tensor used in this work were thus chosen to give approximately the correct condensed phase dipole moment. One of the most encouraging results of the model, however, is that the liquid-phase bond angle and lengths are equivalent to the SPC/F values without any modifications to the intramolecular potential.

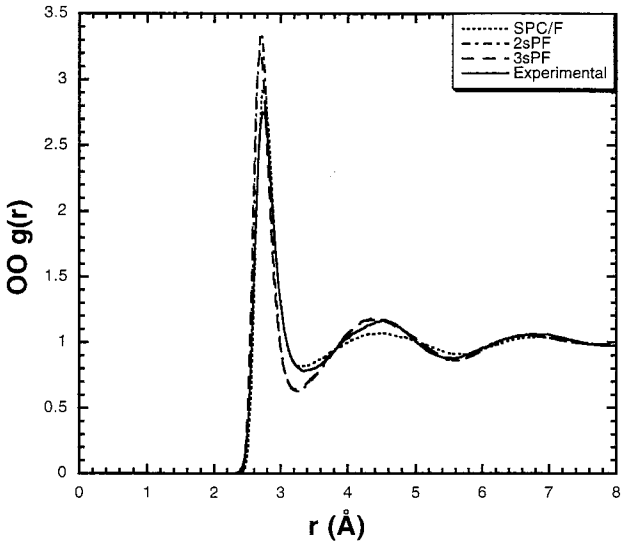

Figure 3. Oxygen−oxygen radial distribution function, $g(r)$, for all three water models: SPC/F (short dash), two-state Polarflex (dot−dash), three-state Polarflex (long dash). The experimental results of Soper are also shown (solid line).

B. Radial Distribution Functions. The radial distribution functions (RDF) for oxygen−oxygen, oxygen−hydrogen, and hydrogen−hydrogen correlations are shown in Figures 3, 4, and 5 for the three theoretical models as well as the experimental result.[30] One-dimensional RDFs such as $g(r)$ give a picture of the average structure in a fluid. It is important to note that these one-dimensional plots are radially averaged and give no information about the anisotropic nature of the liquid structure. In all three plots, the two-state and three-state Polarflex water models give almost indistinguishable results, showing that including polarizability in either one or two directions does not alter the average structural packing in liquid water. The two polarizable models do show a slightly more structured fluid than the nonpolarizable, SPC/F model. This can most likely be attributed to the higher average dipole observed for the polarizable models. In general for the oxygen−oxygen RDF, the SPC/F model exhibits an average structure that is less ordered than the experimental result and the polarizable models show a structure that is slightly more defined than the experimental result, albeit generally in better agreement than the SPC/F model in the second and third solvation shell region.

The oxygen−hydrogen RDF, Figure 4, again shows that the polarizable models result in a slightly more structured fluid than does the SPC/F model. The heightened structure is, however, exaggerated more here than in the oxygen−oxygen RDF. In addition to the peak heights, the peak positions give a qualitative measure of the degree of hydrogen bonding. The Polarflex models have peak positions that are slightly lower than the SPC/F model and experiment. Although this does indicate an

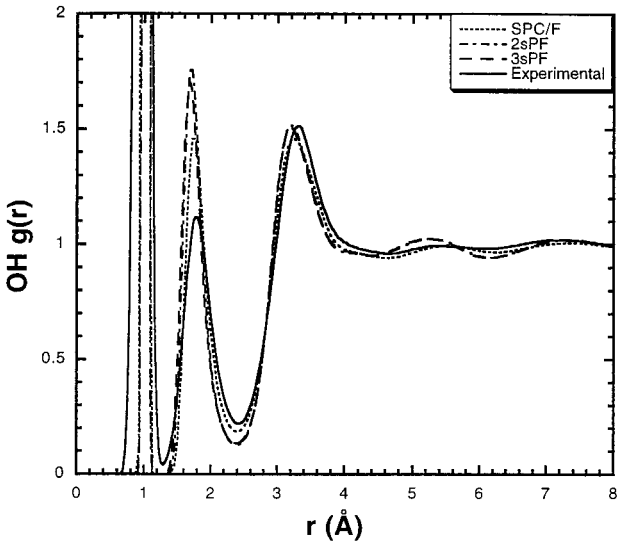

Figure 4. Oxygen−hydrogen radial distribution function, $g(r)$, for all three water models: SPC/F (short dash), two-state Polarflex (dot−dash), three-state Polarflex (long dash). The experimental results of Soper are also shown (solid line).

overbinding in the model, it should be possible to parameterize the model to reduce this slight overbinding. It has also been shown that quantization of water models reduces the degree of hydrogen bonding and therefore reduces the structure of the liquid.[31] Applying quantization through path integral methods to the Polarflex model may therefore yield a result closer to experiment. In addition to the degree of structure, the aforementioned study[31] also showed that quantization reverses the order of the first two peak heights in the oxygen−hydrogen RDF and matches the experimental peak heights better than the classical models did. The effect of nuclear quantization on the Polarflex model will be explored in future work.

Whereas the two-state and three-state models show almost exactly the same average fluid structure, their orientational correlations may differ significantly. An exploration of the way in which the varying of polarizability dimensionality can alter orientational correlations will be the focus of future research.

C. Dielectric Constant. The static dielectric constant, ϵ_0, is the proportionality constant between a material's polarization response to an applied electric field. The value of ϵ_0 is an important measure of an empirical, atomistic potential's accuracy. In continuum-level models, the static dielectric constant is a key property that differentiates one substance from another. Calculating it, however, from atomistic molecular dynamics simulations can be quite difficult due to the fact that it is dependent on the fluctuations in the net system dipole moment, **M**. The net dipole moment for water converges very slowly due to its slow orientational diffusion. The static dielectric constant is defined[32] as

$$\epsilon_0 = \epsilon_\infty + \frac{4\pi\beta}{3V}\langle \mathrm{M}^2\rangle \tag{28}$$

where V is the volume of the simulation cell.

It has been shown that using

$$\langle \mathrm{M}^2\rangle = \langle \mathrm{M}\rangle^2 \tag{29}$$

instead of simply $\langle \mathrm{M}^2\rangle$ in eq 28 can compensate for finite system size effects and result in a quantity that converges more quickly.[33] Formally, $\langle \mathrm{M}\rangle^2$ is zero, but in practice, this is only true after very long simulations. Both methods were employed in order to provide a lower and upper bound for ϵ_0 so as to monitor convergence. An alternative, less computationally intensive, route to the static dielectric constant was proposed by Kusalik and Svishchev.[34] The method may be employed in future work.

The static dielectric constant was calculated for both Polarflex models and compared to the literature value for the SPC/F water model. A total of 100 independent trajectories were run in order to obtain over 5 ns of averaged data for each model. The initial conditions for the trajectories were generated by writing out configuration files once every picosecond from a simulation at 1000 K. These "hot" trajectories were then cooled and allowed to equilibrate for 100 ps before data collection began for the dielectric constant. Samples of the total dipole moment were taken every 10 fs throughout the entirety of the production runs.

The three-state Polarflex water model gives a static dielectric constant of 85 ± 10, whereas the SPC/F model gives a value of 80 ± 10. Both models are adequately in agreement with the experimental value of 78.3. The two-state model exhibits a dielectric constant of 98 ± 10. This difference in dielectric constant is evidence that leaving out nonprincipal degrees freedom can significantly affect a polarizable water model's behavior.

The optical dielectric constant, ϵ_∞, is a measure of a system's instantaneous, electronic response to an electric field. It is unity for a nonpolarizable model, which has no electronic response, and is experimentally a value of 1.79. It is calculated by the expression

$$\epsilon_\infty = 1 + \frac{4\pi}{3V} Tr\{\mathbf{A}\} \tag{30}$$

where **A** is the total, system polarizability tensor.[32] $Tr\{\mathbf{A}\}$ can be approximated with

$$Tr\{\mathbf{A}\} = \sum_{i=1}^{N_{\mathrm{mol}}} Tr\{\boldsymbol{\alpha}_i\} \tag{31}$$

where $\boldsymbol{\alpha}_i$ is the polarizability tensor for molecule i[21] or can be calculated exactly by

$$\mathbf{M}_{\mathrm{tot}} = \mathbf{M}_0 + \mathbf{M}_{\mathrm{ind}} \tag{32}$$

$$\mathbf{M}_{\mathrm{tot}} = \mathbf{M}_0 + \mathbf{A}\cdot\boldsymbol{\epsilon} \tag{33}$$

$$\mathbf{A} = \frac{\mathbf{M}_{\mathrm{tot}} - \mathbf{M}_0}{\boldsymbol{\epsilon}} \tag{34}$$

where $\mathbf{M}_{\mathrm{tot}}$ is the total system dipole moment, $\mathbf{M}_0$ is the total system dipole moment with no electric field present, $\mathbf{M}_{\mathrm{ind}}$ is the electric-field-induced total dipole moment, and $\boldsymbol{\epsilon}$ is an externally applied electric field. Obtaining **A** via eq 34 was accomplished by calculating the total dipole moment of many equilibrated structures with and without an external electric field present. The final **A** was obtained by averaging over these single-point calculations. Note that no simulation is necessary to calculate **A** from eq 31.

We have verified this result and found that both methods yield an ϵ_∞ of 1.23 for the three-state Polarflex model and 1.11 for the two-state Polarflex model. The experimental value is 1.79. Since ϵ_∞ is a direct result of the molecular polarizability tensor, it is not a surprise that it should be too low for the Polarflex models since $\boldsymbol{\alpha}$ does not contain an α_{xx} value. It is a future goal, therefore, to improve the value of ϵ_∞ for the model by including this physical effect. As was mentioned earlier, the

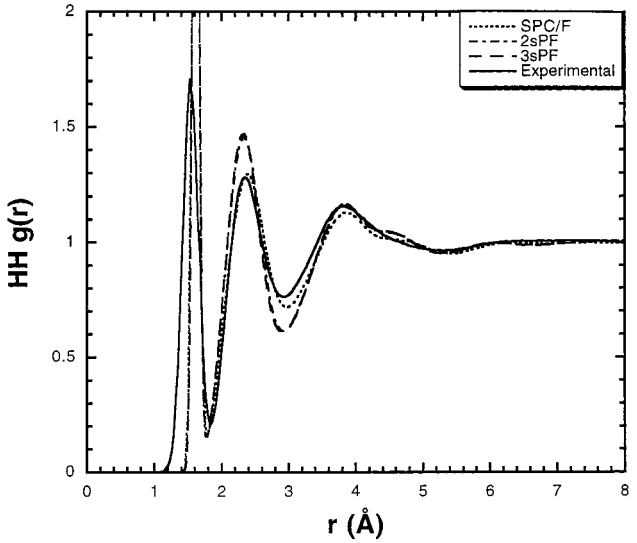

Figure 5. Hydrogen−hydrogen radial distribution function, $g(r)$, for all three water models: SPC/F (short dash), two-state Polarflex (dot−dash), three-state Polarflex (long dash). The experimental results of Soper are also shown (solid line).

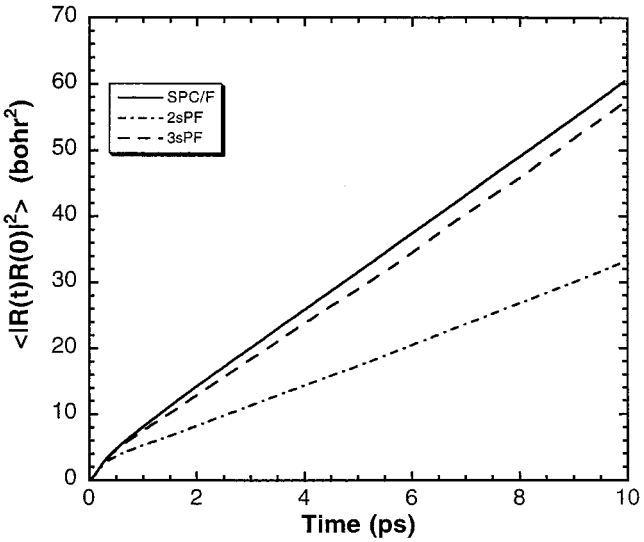

Figure 6. Center of mass, mean-squared displacement for all three water models: SPC/F (solid line), two-state Polarflex (dot−dash), and three-state Polarflex (long dash).

polarizability was also lowered in order to avoid over-polarization of the system in the condensed phase. While the MS-EVB nature of the Polarflex model prevents "polarization catastrophes", it is possible that the strong interactions between the close-range point charges induce an overpolarization. The addition of either a short-range Coulombic cutoff or the use of Gaussian charge distributions instead of point charges may allow something closer to the experimental polarizability tensor to be used and could result in a more accurate optical dielectric constant. Other models that do not have fully isotropic polarizability also exhibit a low ϵ_∞ value,[35] but despite this shortcoming, the present model is a step better than using the nonpolarizable value of unity.

D. Dynamical Properties. *1. Self-Diffusion Constant.* The Einstein relationship,

$$\frac{\mathrm{d}}{\mathrm{d}t}\Delta R^2(t) = 6D \tag{35}$$

provides a common theoretical pathway to the self-diffusion constant. Figure 6 shows the mean squared displacement time correlation function (TCF) for the three water models. Simple linear regression fits were performed on each series to obtain the diffusion constants listed in Table 5. The positions were sampled every 50 ps throughout the simulation.

The SPC/F model was parameterized to give a diffusion constant close to the experimental value, so it is not surprising that $D = 3.0 \times 10^{-9}$ m^{2}s^{-1} for this model. The three-state Polarflex model exhibits a slightly slower mean squared displacement over time, which can be attributed to the higher average dipole moment and thus higher degree of structure in the liquid. It is quite interesting, however, that the two-state Polarflex model, with the same average dipole moment and binding energy as the three-state model, gives a mean-squared displacement over time that is much lower than either of the other two models. The restriction of the polarizability to a single direction evidently has a significant impact on the self-diffusion constant.

Quantum effects may also have a significant impact on the self-diffusion constant,[31] increasing its value by as much as 50%. As such, one might expect the three-state Polarflex model to come into better agreement with experiment upon quantization, and this will be the subject of future research.

2. Infrared Absorption Spectrum. The infrared power spectrum can be calculated from simulation results in a number of ways. In a constant-partial-charge simulation, the Fourier transform of the velocity autocorrelation function gives a good approximation. This approach leaves out, however, the time-dependent contributions from the changing charges in a polarizable model, as shown by the expression

$$\boldsymbol{\mu} = \sum_{i=1}^{M} q_i \mathbf{r}_i$$

$$\frac{\partial \boldsymbol{\mu}}{\partial t} = \sum_{i=1}^{M}\left[\frac{\partial q_i}{\partial t}\mathbf{r}_i + q_i \mathbf{v}_i\right] \tag{36}$$

where M is the number of atoms per molecule. The power spectrum has therefore been calculated via the expression

$$I(\omega) \cong \frac{1}{2\pi}\int_{-\infty}^{+\infty} \mathrm{d}t \mathrm{e}^{-i\omega t} \sum_{i=1}^{N_{\mathrm{mol}}} \left\langle \frac{\partial \boldsymbol{\mu}_i}{\partial t}(t)\frac{\partial \boldsymbol{\mu}_i}{\partial t}(0)\right\rangle \tag{37}$$

where $\langle \partial\mu_i(t)/\partial t \partial\mu_i(0)/\partial t\rangle$ is the individual molecular dipole time derivative autocorrelation function. Note that cross-correlations have been neglected in this expression—an approximation which is reasonable for the intramolecular vibrations. The autocorrelation function was calculated during the course of the simulation every 1 fs of a 50 ps production run that had already been equilibrated to 300 K. No thermostat was used in order to preserve the integrity of the time correlation function. Figures 7 and 8 show the infrared spectrum for the three water models. For an alternative calculation of the spectrum, see refs 36 and 37.

The SPC/F intramolecular potential is not explicitly dependent on the partial charges of the nuclear sites, and so the differences seen in Figure 7 in the three models are a result of the different Coulombic forces experienced by the individual atoms. In general, the two polarizable models give broader, and sometimes more split, peaks than does the SPC/F, nonpolarizable model. Table 6 gives the dominant frequencies for the three, intramolecular vibrations in water for the three models, as well as the gas-phase values for the theoretical models and experimental,

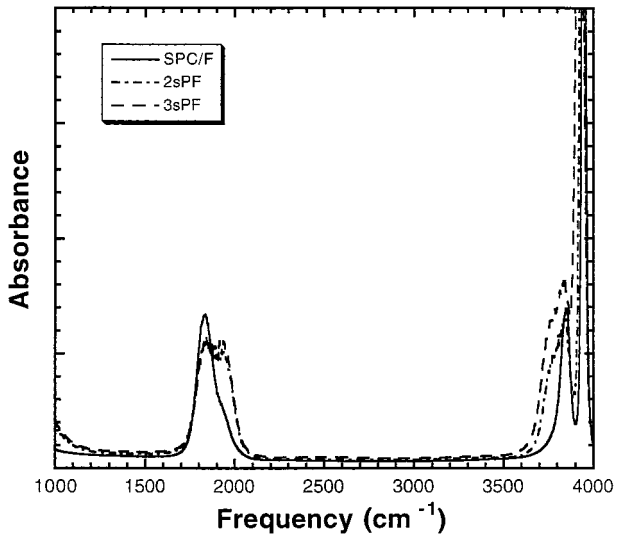

Figure 7. Infrared spectra for the three water models: SPC/F (solid line), two-state Polarflex (dot−dash), three-state Polarflex (long dash).

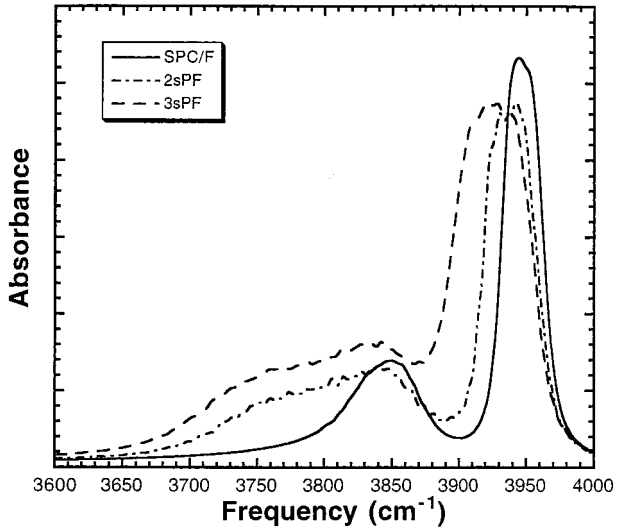

Figure 8. Enlarged view of the high-frequency infrared spectra for the three water models: SPC/F (solid line), two-state Polarflex (dot−dash), three-state Polarflex (long dash).

TABLE 6: Intramolecular Vibrational Frequencies (cm^{-1})

	bending	symmetric stretch	asymmetric stretch
experiment gas phase[a]	1595	3657	3756
SPC/F, 2S−PF, 3S−PF gas phase	1649	3832	3942
expt liquid phase[b]	1645	3280	3490
SPC/F	1832	3848	3945
2S−PF	1892	3830	3935
3S−PF	1892	3830	3925

[a] Reference 47. [b] Reference 48.

condensed phase results. The gas-phase values are the original SPC/F input parameters.

While the Polarflex models do not change the vibrational spectrum significantly, there are some interesting features. Just as in the experimental values, a significant blue shift is observed in the condensed phase bending vibration relative to the gas-phase value, and this is more pronounced in the polarizable models. The condensed phase red-shift seen in the experimental O−H stretching spectrum (~400 cm^{-1}) is observed to be only about 10 cm^{-1} in the polarizable models and not at all for SPC/F. The inability of the current models to reproduce this feature is likely due to the quadratic form of the intramolecular potential used in eq 2, since the actual red shift is caused by the anharmonicity of the bonds. This will be a target for improvement in future work, and the inclusion of quantum red-shift effects will also be important.

VI. Concluding Remarks

A simple polarizable and flexible water potential, called Polarflex, has been developed in this work using the MS-EVB method. A two-state Polarflex model that is polarizable only in the principal axis direction has been shown to give reasonable average properties, but it suffers from a low diffusion constant and high static dielectric constant, ϵ_0. A more realistic model, having polarizability along both axes in the molecular plane, has also been tested that gives the same average dipole, binding energy, and molecular geometry as the simpler model, but exhibits diffusion and dielectric constants that are in better agreement with experiment. By design, the monomer dipole exactly matches the experimental result, but the dimer oxygen−oxygen distance and energy are much closer to the experimental values than the nonpolarizable SPC/F model. All of these results suggest that Polarflex may be a more physically reasonable water potential for, e.g., heterogeneous or interfacial simulations.

The two Polarflex models exhibit nearly identical radial distribution functions (RDFs) and, in general, show a slightly more structured fluid than does the nonpolarizable, SPC/F model. The Polarflex models are thus more ordered than is the experimental result, but are still a reasonable approximation to the real fluid. The liquid state bond angle and bond lengths for the Polarflex models are comparable with SPC/F and other water models that are in use. The infrared vibrational spectrum changed only slightly in going from the nonpolarizable to the polarizable model, but in general the addition of polarizability broadened the absorption lines. The Polarflex models showed a slight blue shift in the bending peak and a small red shift in the OH vibrational peaks.

Computationally, Polarflex water is about four times slower than nonpolarizable water, but the application of the extended Lagrangian method[3,20,38] and a multiple time step algorithm could speed up Polarflex considerably. This would make the model more useful for large, biomolecular simulations for example. Work is in progress to improve the realism of the polarizability tensor and therefore the value of ϵ_∞, by using Gaussian-smeared charges instead of point charges. A flexible and polarizable model based on the TIP5P potential[39] as well as the incorporation of the Polarflex water model into the multistate MS-EVB approach for proton transport are also being explored.

Acknowledgment. This research was inspired by the pioneering contributions of Bruce Berne to the field of theoretical chemistry and, in particular, by his development of novel polarizable models for water. The authors also thank Udo Schmitt, Gary Ayton, Kurt Glaesemann, Hyung Kim, and Charles Schwieters for helpful discussions. This work was supported by the Department of Energy Office of Basic Energy Sciences. An allocation of computer time from the Center for High Performance Computing at the University of Utah is gratefully acknowledged.

Appendix A: Implementation of the Ewald Summation in Polarflex

The Ewald summation technique was utilized to calculate the long range potentials and forces. The method assumes that the

system is infinitely periodic in all directions and calculates the Coulomb interactions over all cells via a Fourier-space summation. The resulting sum over all boxes of length L, given by

$$V_{\text{Coulomb}} = V_{\text{RSpace}} + V_{\text{KSpace}} \tag{A1}$$

is conditionally convergent and is given by a real-space summation over all sites, N_s, in the central simulation cell, i.e.,

$$V_{\text{RSpace}} = \sum_{i=1}^{N_s-1}\sum_{j>i}^{N_s} q_i q_j \frac{erfc(\kappa|\mathbf{r}_{ij}|)}{|\mathbf{r}_{ij}|} \tag{A2}$$

and a k-space summation over all other cells, i.e.,

$$V_{\text{KSpace}} = \frac{4\pi}{2V}\sum_{|\mathbf{k}|\neq 0}^{\mathbf{k}_{\max}} \frac{e^{-|\mathbf{k}|^2/4\kappa^2}}{|\mathbf{k}|^2}\{[\sum_{i=1}^{N_s}\sum_{j=1}^{N_s} q_i q_j e^{i\mathbf{k}\cdot\mathbf{r}_{ij}}] - V_{\text{ionicSelf}} - V_{\text{MolecSelf}}\} \tag{A3}$$

where

$$V_{\text{IonicSelf}} = \frac{\kappa}{\sqrt{\pi}}\sum_{i=1}^{N_s} q_i^2 \tag{A4}$$

and

$$V_{\text{MolecSelf}} = \sum_{i=1}^{M-1}\sum_{j=n+1}^{M} \frac{q_i q_j erf(\kappa|\mathbf{r}_{ij}|)}{|\mathbf{r}_{ij}|} \tag{A5}$$

Here, M is the number of atoms per molecule, and $\mathbf{k} = 2\pi\mathbf{n}/L$, where the components of $\mathbf{n}$ are integers from $0 \rightarrow n^{\max}$. The wave vector $\mathbf{k}_{\max}$ is formally infinity, but in this simulation $n_{x,y,z}^{\max} = 8$ combined with $n_{\max}^2 = 54$ gave a converged result. The notation $erf(\cdots)$ and $erfc(\cdots)$ refer, respectively, to the error function and complimentary error function. The Gaussian spreading factor, κ, was set to 6.4/L. Note that the real-space summation does not include intramolecular interactions, but the Fourier-space summation does include all interactions (and subsequently removes the erroroneous intramolecular ones).

The expression for the Coulombic force on atom i, derived from eqs A2−A5, is

$$\mathbf{F}_i = \mathbf{F}_{\text{RSpace}} - \mathbf{F}_{\text{KSpace}} - \mathbf{F}_{\text{MolecSelf}} \tag{A6}$$

where

$$\mathbf{F}_{\text{RSpace}} = \sum_{j\neq i}^{N_s} \frac{q_i q_j}{|\mathbf{r}_{ij}|^3}\mathbf{r}_{ij}\left[erfc(\kappa|\mathbf{r}_{ij}|) + \frac{2\kappa}{\sqrt{\pi}}|\mathbf{r}_{ij}|e^{-(\kappa|\mathbf{r}_{ij}|)^2}\right] \tag{A7}$$

$$\mathbf{F}_{\text{KSpace}} = \frac{4\pi}{V}\sum_{|\mathbf{k}|\neq 0}^{\mathbf{k}_{\max}} \frac{e^{-|\mathbf{k}|^2/4\kappa^2}}{|\mathbf{k}|^2}\mathbf{k}[q_i F\{(\sum_{j=1}^{N_s} q_j e^{i\mathbf{k}\cdot\mathbf{r}_j})e^{-i\mathbf{k}\cdot\mathbf{r}_j}\}] \tag{A8}$$

and

$$\mathbf{F}_{\text{MolecSelf}} = \sum_{j\neq i}^{M} \frac{q_i q_j}{|\mathbf{r}_{ij}|^3}\mathbf{r}_{ij}\left[\frac{2\kappa}{\sqrt{\pi}}|\mathbf{r}_{ij}|e^{-(\kappa|\mathbf{r}_{ij}|)^2} - erfc(\kappa|\mathbf{r}_{ij}|)\right] \tag{A9}$$

In eq A8, $F\{\cdots\}$ refers to the imaginary part of $\{\cdots\}$.

The Polarflex algorithm requires the Coulombic potential energy contribution of each water molecule in each EVB charge state, but the method depicted in eqs A2−A5 gives only the total Coulombic potential energy. This task is cleanly accomplished with only a single Ewald summation for each solution iteration by calculating the electrostatic potential at each atomic site and then later multiplying by the site charge for each EVB state (see eqs 24 and 25). A slight modification was therefore made to eqs A2−A5 in order to calculate the EP at each atomic site without increasing the computational complexity of the summation. This modified sum for the calculation of the EP at atomic site i is given by

$$\text{EP}_i = \text{EP}_i^{\text{RSpace}} + \text{EP}_i^{\text{KSpace}} \tag{A10}$$

where

$$\text{EP}_i^{\text{RSpace}} = \sum_{j\neq i}^{N_s} q_j \frac{erfc(\kappa|\mathbf{r}_{ij}|)}{|\mathbf{r}_{ij}|} \tag{A11}$$

and

$$\text{EP}_i^{\text{KSpace}} = \sum_{\mathbf{k}\neq 0}^{\mathbf{k}_{\max}} W_1(\mathbf{k})W_2(\mathbf{k})e^{-i\mathbf{k}\cdot\mathbf{r}_j} \tag{A12}$$

The term

$$W_1(\mathbf{k}) = \frac{4\pi}{V}\frac{e^{-|\mathbf{k}|^2/4\kappa^2}}{|\mathbf{k}|^2} \tag{A13}$$

is calculated only once per timestep, and

$$W_2(\mathbf{k}) = \sum_{j=1}^{N_s} q_j e^{i\mathbf{k}\cdot\mathbf{r}_j} \tag{A14}$$

is computed once per SCF iteration. The Coulombic potential energy contribution of a particular molecule, I, in EVB state $|n\rangle$, is recovered by

$$V_I^n = [\sum_{i=1}^{M} q_i^n \text{EP}_i^{\text{RSpace}} + q_i^n \text{EP}_i^{\text{KSpace}} - V_{\text{IonicSelf}}] - V_{\text{MolecSelf}} \tag{A15}$$

where

$$V_{\text{IonicSelf}} = \frac{\kappa}{\sqrt{\pi}} q_i^n q_i \tag{A16}$$

and

$$V_{\text{MolecSelf}} = \sum_{i=1}^{M-1}\sum_{j=i+1}^{M} (q_i^n q_j + q q_{ij}^n)\frac{erf(\kappa|\mathbf{r}_{ij}|)}{|\mathbf{r}_{ij}|} \tag{A17}$$

Note that q_i^n is the charge on site i in MS-EVB state $|n\rangle$ and q_i is the expectation value for the charge on site i. The term V_I^n is added to each diagonal, gas-phase element in molecule I's Hamiltonian matrix (see eq 24), the matrices are diagonalized, charges are determined, and the process is iterated until convergence is obtained. Note that no force calculation is necessary until after the charges have been determined.

References and Notes

(1) Toukan, K.; Rahman, A. *Phys. Rev. B* **1985**, *31*, 2643.
(2) Dang, L. X.; Pettitt, B. M. *J. Chem. Phys.* **1987**, *91*, 3349.
(3) Rick, S. W.; Stuart, S. J.; Berne, B. J. *J. Chem. Phys.* **1994**, *101*, 6141.
(4) Borgis, D.; Staib, A. *Chem. Phys. Lett.* **1995**, *238*, 187.
(5) Bursulaya, B. D.; Kim, H. J. *J. Chem. Phys.* **1998**, *108*, 3277.

(6) Sprik, M.; Klein, M. L. *J. Chem. Phys.* **1988**, *89*, 7556.
(7) Sprik, M. *J. Phys. Chem.* **1991**, *95*, 2283.
(8) Zhu, S. B.; Yao, S.; Zhu, J. B.; Singh, S.; Robinson, G. W. *J. Phys. Chem.* **1991**, *95*, 6211.
(9) Zhu, S.-B.; Singh, S.; Robinson, G. W. *J. Chem. Phys.* **1991**, *95*, 2791.
(10) Stillinger, F. H. *J. Chem. Phys.* **1979**, *71*, 1647.
(11) Stillinger, F. H.; David, C. W. *J. Chem. Phys.* **1978**, *69*, 1473.
(12) Corongiu, G.; Clementi, E. *J. Chem. Phys.* **1993**, *98*, 4984.
(13) Schmitt, U.; Voth, G. A. *J. Phys. Chem.* **1998**, *102*, 5547.
(14) Schmitt, U. W.; Voth, G. A. *J. Chem. Phys.* **1999**, *111*, 9361.
(15) Vuilleumier, R.; Borgis, D. *J. Mol. Struct.* **1998**, *436*, 555.
(16) Koji, A.; Hynes, J. T. *Adv. Chem. Phys.* **1999**, *110*, 381.
(17) Mulliken, R. *J. Chim. Phys.* **1964**, 61.
(18) Warshel, A.; Weiss, R. *J. Am. Chem. Soc.* **1980**, *102*, 6218.
(19) Chang, Y.; Miller, W. *J. Phys. Chem.* **1990**, *94*, 5884.
(20) Rick, S. W.; Cachau, R. E. *J. Chem. Phys.* **2000**, *112*, 5230.
(21) Bursulaya, B. D.; Jeon, J.; Zichi, D. A.; Kim, H. J. *J. Chem. Phys.* **1998**, *108*, 3286.
(22) Bursulaya, B. D.; Kim, H. J. *J. Chem. Phys.* **1998**, *109*, 4911.
(23) Bursulaya, B. D.; Kim, H. J. *J. Chem. Phys.* **1999**, *110*, 9646.
(24) Bursulaya, B. D.; Kim, H. J. *J. Chem. Phys.* **1999**, *110*, 9565.
(25) Shepard, A. C.; Beers, Y.; Klein, G. P.; Rothman, L. S. *J. Chem. Phys.* **1973**, *59*, 2254.
(26) Murphy, W. F. *J. Phys. Chem.* **1977**, *67*, 5877.
(27) Allen, M. P.; Tildesley, D. J. *Computer Simulation of Liquids*; Oxford University Press: New York, 1987.
(28) Ewald, P. *Ann. Phys.* **1921**, *64*, 253.
(29) Leeuw, S. W. D.; Perram, J. W.; Smith, E. R. *Proc. R. Soc. London* **1983**, *388*, 177.
(30) Soper, A. K. *Chem. Phys.* **2000**, *258*, 121−137.
(31) Lobaugh, J.; Voth, G. A. *J. Chem. Phys.* **1997**, *106*, 2400.
(32) Neumann, M.; Steinhauser, O. *Chem. Phys. Lett* **1984**, *106*, 563.
(33) Wei, D.; Patey, G. N. *Phys. Rev. A* **1992**, *46*, 7783.
(34) Kusalik, P. G.; Mandy, M. E.; Svishchev, I. M. *J. Chem. Phys.* **1994**, *100*, 7655−7664.
(35) Bader, J. S.; Cortis, C. M.; Berne, B. J. *J. Chem. Phys.* **1997**, *106*, 2372.
(36) Reimers, J. R.; Watts, R. O. *Chem. Phys.* **1984**, *91*, 201−223.
(37) Reimers, J. R.; Watts, R. O. *Chem. Phys. Lett.* **1983**, *94*, 222−226.
(38) Belle, D. V.; Frieyen, M.; Lippens, G.; Wodak, S. *J. Mol. Phys.* **1992**, *77*, 239−255.
(39) Mahoney, M. W.; Jorgensen, W. L. *J. Chem. Phys.* **2000**, *112*, 8910.
(40) Benedict, W. S.; Gailar, N.; Plyler, E. K. *J. Chem. Phys.* **1965**, *24*, 1139.
(41) Odutola, J. A.; Dyke, T. R. *J. Chem. Phys.* **1980**, *72*, 5062.
(42) Jorgensen, W. L.; Chandrasekhar, J.; Madura, J.; Impey, R. W.; Klein, M. L. *J. Chem. Phys.* **1983**, *79*, 926.
(43) Coulson, C. A.; Eisenburg, D. *Proc. R. Soc. London Ser. A* **1966**, *291*, 454.
(44) Ichikawa, K.; Kameda, Y.; Yamaguchi, T.; Wakita, H. *Mol. Phys.* **1991**, *73*, 74.
(45) Buckingham, A. D. *Proc. R. Soc. London Ser. A* **1956**, *238*, 235.
(46) Krynicki, K.; Green, C. D.; Sawyer, D. W. *Discuss. Faraday Soc.* **1978**, *66*, 199.
(47) Benedict, W. S.; Gailar, N.; Plyler, E. K. *J. Chem. Phys.* **1956**, *24*, 1139.
(48) Bayly, J. G.; Kartha, V. B.; Stevens, W. H. *Infrared Phys.* **1963**, *3*, 211.